NANO · MICRO small
www.small-journal.com

Healable, Recyclable, and Multifunctional Soft Electronics Based on Biopolymer Hydrogel and Patterned Liquid Metal

Xing Peng Hao, Chuan Wei Zhang, Xin Ning Zhang, Li Xin Hou, Jian Hu, Michael D. Dickey,* Qiang Zheng, and Zi Liang Wu**

Recent years have witnessed the rapid development of sustainable materials. Along this line, developing biodegradable or recyclable soft electronics is challenging yet important due to their versatile applications in biomedical devices, soft robots, and wearables. Although some degradable bulk hydrogels are directly used as the soft electronics, the sensing performances are usually limited due to the absence of distributed conducting circuits. Here, sustainable hydrogel-based soft electronics (HSE) are reported that integrate sensing elements and patterned liquid metal (LM) in the gelatin–alginate hybrid hydrogel. The biopolymer hydrogel is transparent, robust, resilient, and recyclable. The HSE is multifunctional; it can sense strain, temperature, heart rate (electrocardiogram), and pH. The strain sensing is sufficiently sensitive to detect a human pulse. In addition, the device serves as a model system for iontophoretic drug delivery by using patterned LM as the soft conductor and electrode. Noncontact detection of nearby objects is also achieved based on electrostatic-field-induced voltage. The LM and biopolymer hydrogel are healable, recyclable, and degradable, favoring sustainable applications and reconstruction of the device with new functions. Such HSE with multiple functions and favorable attributes should open opportunities in next-generation electronic skins and hydrogel machines.

1. Introduction

Soft electronics offer promising applications in health monitoring,[1] wearable electronics,[2] soft robotics,[3] and human–machine interfaces.[4] To devise such soft electronics, stretchable conductors with high conductivity and easy-integration with elastomeric substrates are highly desired and recognized as important cornerstones. There are generally two strategies to impart conductors with desirable stretchability. The first strategy is to develop intrinsic stretchable conductors such as by incorporating conducting fillers into elastomers[5,6] or ionic salts into gels.[7,8] However, their conductivity is relatively low and changes (often drastically) during stretching, resulting in reduced performances and limiting applications.[9] Another strategy for stretchable conductors is through structure engineering of rigid conducting materials.[10] For example, thin metal films are geometrically designed with serpentine, buckle, or ring shapes to afford additional stretchability through local flexing. However, the stretchability of these conductors is limited to two to three times their original length, and the modulus-mismatch between the rigid conductor and soft substrate may cause failure. Recently, gallium-based room-temperature liquid metals (LMs) have been demonstrated as ideal conductors for soft electronics due to the metallic conductivity, unlimited deformability, and low-toxicity.[11–17] Various soft electronics are devised by incorporating LM into elastomers (e.g., polydimethylsiloxane [PDMS]), which usually have relatively high modulus (>2 MPa) compared to soft biotissues (<200 kPa), and relatively poor permeability to water and hydrophilic solutes. Furthermore, elastomers such as PDMS are usually not degradable nor recyclable.[18] These attributes have environmental implications and limit the application of soft electronics in biomedical fields in which biocompatibility, biodegradability, and permeability of nutrients are essential concerns.

Hydrogels share similarities with soft biotissues. Thus, these hydrophilic networks are an intriguing substrate for soft electronics that interact with the human body.[19–23] Although many synthetic hydrogels exist with remarkable mechanical properties, they are often not degradable nor safe to interact with the human body. Synthesis of robust yet degradable/recyclable hydrogels from biopolymers, especially through facile strategies, is highly desired for the development of hydrogel-based soft electronics (HSE).[24] In actual, some bulk hydrogels are applied to devise HSE by incorporating salts, carbon nanotubes, silver nanowires, or conducting polymers into the gel matrix.[8,19,20] However, owing to the poor conductivity, it is

X. P. Hao, C. W. Zhang, X. N. Zhang, L. X. Hou, Q. Zheng, Z. L. Wu
Ministry of Education Key Laboratory of Macromolecular Synthesis and Functionalization
Department of Polymer Science and Engineering
Zhejiang University
Hangzhou 310027, China
E-mail: wuziliang@zju.edu.cn

J. Hu
State Key Laboratory for Strength and Vibration of Mechanical Structures
Department of Engineering Mechanics
Xi'an Jiaotong University
Xi'an 710049, China
E-mail: hujian@mail.xjtu.edu.cn

M. D. Dickey
Department of Chemical and Biomolecular Engineering
North Carolina State University
Raleigh, NC 27695, USA
E-mail: mddickey@ncsu.edu

The ORCID identification number(s) for the author(s) of this article can be found under https://doi.org/10.1002/smll.202201643.

DOI: 10.1002/smll.202201643

difficult to pattern the conductive element as integrated sensing units in one hydrogel device for multiple sensing functions. On the other hand, there are few reports on soft electronics by integrating stretchable conductors or sensing elements with biopolymer hydrogels, although many biopolymer gels possess notable degradability, self-healing ability, and/or adhesiveness.[25,26] We envision to devise multifunctional soft electronics by patterning LM on biopolymer hydrogel as conductive interconnects to sensing units. LM is orders of magnitude more conductive than hydrogels[15] and therefore offers benefits relative to approaches that utilize hydrogel as conductors or sensing components.

We report here a series of multifunctional soft electronics by integrating patterned LM and sensing elements into robust biopolymer hydrogels. The hydrogel substrate is developed by temperature-mediated sol–gel transition of the aqueous mixture of gelatin and alginate with hydrogen and ionic bonding, which can be further toughened by calcium ions to form chelate interactions with the alginate. The gallium-based LM is patterned on the hydrogel substrate through stencil printing. The resultant devices exhibit high sensitivity to mechanical strain, which can be used to detect tiny motions of a human being. The high conductivity and good patternability of LM enable the fabrication of multifunctional HSE by integrating sensing units to detect vital biophysical information. Local iontophoretic drug delivery can also be realized using the LM electrodes in the HSE. Moreover, the HSE with an array of LM-based electrodes is capable of noncontact perception of nearby objects based on electrostatic-field-induced voltage, which should be useful for soft robotic sensing of objects. Another important attribute of this HSE is the healable, degradable, and recyclable hydrogel substrate, favoring the reuse and reconstruction of the device with new functions. To our best knowledge, such HSE with features of easy-fabrication, low-cost, and multifunction is rarely reported, despite of many achievements in other HSE (Table S1, Supporting Information). This work should merit the design of other HSE and promote the applications in biomedical and engineering fields.

2. Results and Discussion

2.1. Fabrication and Generic Features of HSE

Our HSE has two primary components: the robust yet degradable biopolymer hydrogel as the substrate and stretchable patterned LM as the conductor, as illustrated in **Figure 1**a. The biopolymer hydrogels are facile to prepare by sol–gel transition of the mixture solution of gelatin and alginate (Figure 1b; see details in Experimental Section). Briefly, the helix–helix association of gelatin polymer chains results in gelation of the solution when cooled down from relatively high temperature. To create gels suitable for different applications, we have prepared two kinds of hydrogels through different protocols (Figure 1c,d).

The first kind of hydrogel consists of gelatin and alginate with water and glycerol as the mixed solvent (Figure 1c). These gelatin–alginate–glycerol (GA) hydrogels are denoted as GA-f_x-f_y-f_z, where f_x, f_y, and f_z represent the weight percentage (wt%; relative to the hydrogel) of gelatin, alginate, and glycerol, respectively. The recipes of precursor solutions for the synthesis of hydrogels are listed in Table S2, Supporting Information. Gelatin with helix–helix association serves as the main network and determines the mechanical properties of the hydrogels. However, the relatively low melting point (33.4 °C) of gelatin hydrogels hampers their application as substrates for soft electronics when used on/in the human body (Figure S1, Supporting Information). The addition of glycerol and alginate increases the thermal and mechanical stability of gelatin-based hydrogels by enhanced intra-/inter-molecular hydrogen and ionic bonds (Figure S2, Supporting Information).[27] The resultant hydrogels are transparent, resilient, healable, self-adhesive, and durable, which are ideal substrate materials for electronic skins (Figure 1e and Figure S3, Supporting Information). Another attractive feature of the biopolymer hydrogels is the biodegradability, which is important for the design of transient HSE in biomedical applications. As shown in Figure 1f, the disc-shaped hydrogel completely biodegrades in gelatin hydrolase solution (GHS) at room temperature within 10 h.

The second kind of hydrogel is prepared for the design of underwater or implantable electronics (Figure 1d,g). By subsequent physical cross-linking of alginate network with calcium ions (Ca^{2+}), the degradation rate of the hydrogel slows significantly to afford a stable performance in aqueous environments. The hydrogels maintain constant dimensions after incubation in water, GHS, and phosphate buffered saline (PBS) for 7 days (Figure S4, Supporting Information). We note that the all the components of our hydrogels are naturally occurring materials, which are safe, high-biocompatible, eco-friendly, and even edible.[28–30]

For the stretchable conductor of HSE, we choose eutectic gallium–indium (EGaIn) alloy (melting point: 16 °C) which has high conductivity and deformability. However, it is difficult to print EGaIn alloy on the surface of hydrogels due to the poor adhesion.[31] To improve the printability, 25 wt% of iron particles (Fe; mean diameter, 5 μm) are added to the EGaIn alloy. The resultant Fe-EGaIn amalgam has high conductivity (2×10^5 S m^{-1}), good adhesiveness, and printability on various materials.[32] Diverse conductive patterns can be facilely created on different substrates by stencil printing (Figure S5, Supporting Information). HSE is thus obtained by integrating the degradable biopolymer hydrogel with the patterned LM, which can withstand large-amplitude bending and stretching without losing its structural integrity and electric functions (Figure 1h).

2.2. Tunable Properties of Biopolymer Hydrogels

As important features for soft electronics, high stretchability, resilience, and durability are highly desired but such properties are often deficient in biopolymer hydrogels. Tunable mechanical properties of the hydrogel substrates are also enticing for soft electronics to satisfy different application scenarios. These demands can be readily met in these gelatin–alginate hydrogels with tailored mechanical performances by adjusting the content of gelatin or glycerol, corresponding to the variations of polymer fraction and/or the density of physical cross-links.[27,33] When the content of gelatin (f_x) increases from 5 to 25 wt%, while keeping the contents of alginate (f_y) and glycerol (f_z) as

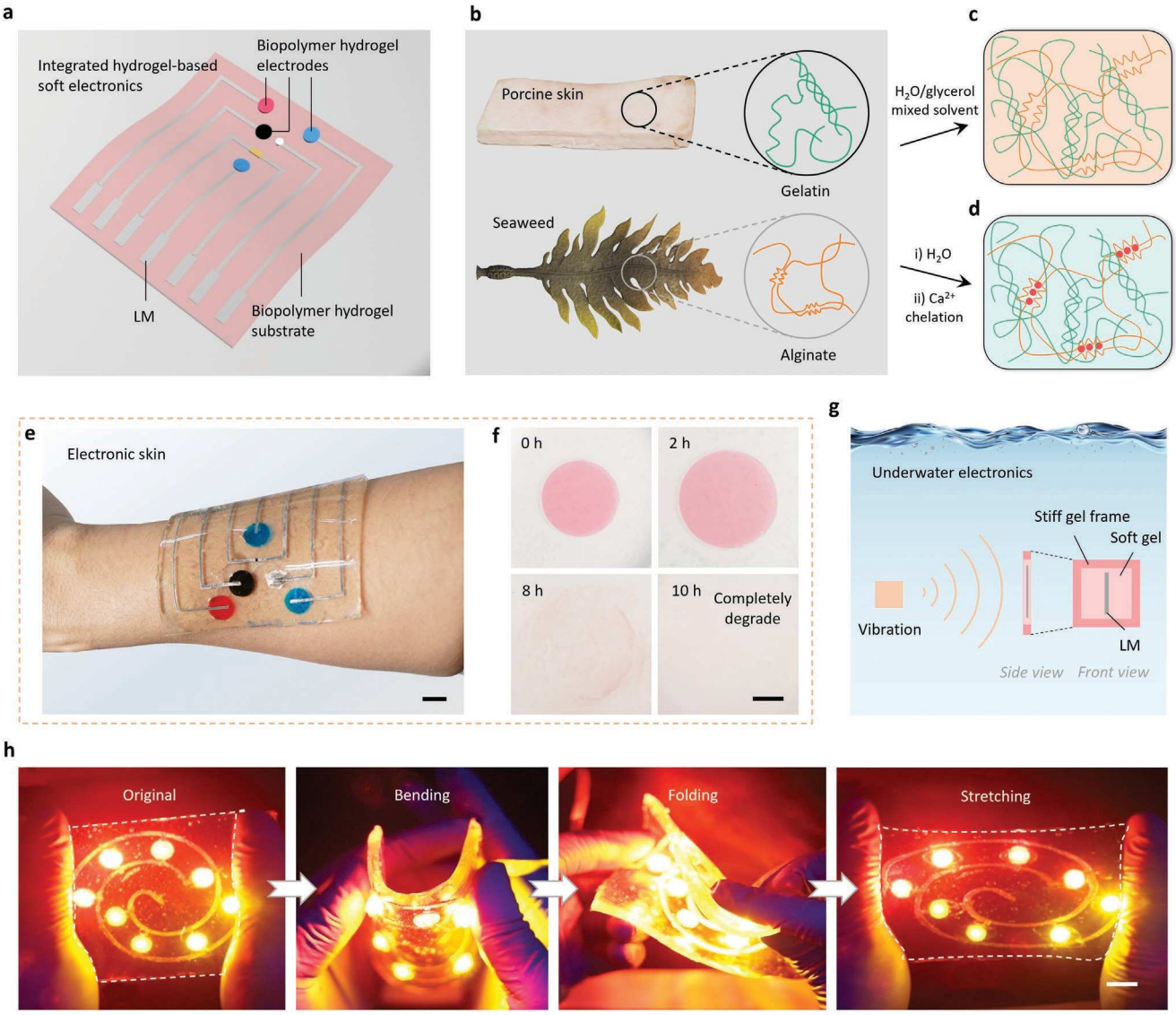

Figure 1. Fabrication of robust biopolymer hydrogels as the substrate of soft electronics. a) Illustration of integrated soft electronics with biopolymer gel as the substrate. b–d) Biopolymer hydrogels made of gelatin and alginate (b) with water and glycerol as mixed solvent to form robust hydrogels cross-linked by polymer chain entanglement, and hydrogen, ionic bonding (c) or further cross-linked by Ca^{2+} ions to chelate with the alginate (d). e) Application of gelatin–alginate–glycerol hydrogel with patterned LM and sensing units as electronic skins. f) Enzymatic biodegradation process of the hydrogel in gelatin hydrolase solution at 22 °C. g) Schematic for the application of the soft electronics with Ca^{2+}-cross-linked hydrogel as underwater electronics to detect the vibration of objects. h) Biopolymer hydrogel-based soft electronics with spiral LM circuits and light-emitting diode (LED) array in the original, bending, twisting, and stretching states. Scale bars = 1 cm.

1.5 and 16 wt%, respectively, the Young's modulus (E) and breaking strain (ε_b) of the GA hydrogels increase from 16 to 123 kPa and from 126% to 314% (**Figure 2**a,b), which cover the range of E (20–200 kPa) and deformation ratio (<30%) of most biotissues. E and ε_b of the hydrogel can be further increased to 0.5 MPa and 530%, respectively, when f_x is increased to 50 wt% (Figure S6, Supporting Information). Yet, this complicates the fabrication process because of the ultrahigh viscosity of the precursor solution. Alternatively, tough biopolymer hydrogels with desirable water content can be obtained by solvent evaporation at room temperature, which will be described later.

Despite having high stretchability, our biopolymer hydrogels possess excellent resilience. Under cyclic stretching with the maximum strain of 100%, the hydrogel (GA-20-1.5-16) shows linear stress–strain curves and small hysteresis with constant energy dissipation (≈13%) (Figure 2c). After 50 loading–unloading cycles, no obvious decrease in elasticity is observed in the hydrogel. A small residual strain (≈10%) is found in the hydrogel after cyclic stretching, which may come from the slightly dehydration of the gel in air. The good resilience of the biopolymer hydrogel promises high mechanical and electrical stability of the HSE under repeated deformation.

The problem of dehydration in air can be partially mitigated by increasing the content of glycerol (f_z), which also results in the improvement of mechanical properties of the gels. As shown in Figure 2d, E and ε_b of the hydrogels (GA-20-1.5-f_z)

increase from 54.7 to 115.1 kPa and from 209% to 446%, respectively, with the increase in f_z from 0 to 48 wt%, because of the enhanced hydrogen bond associations.[33] Considering the mechanical properties, processability, and sol–gel transition temperature, GA-20-1.5-16 and GA-20-1.5-32 hydrogels are appropriate substrate to devise electronic skins. When the GA hydrogel (GA-20-1.5-32) is placed in air at room temperature with relative humidity (RH) of 20%, E and ε_b of the gel increase with the time (Figure 2e), which is consistent with the varied mechanical properties of the hydrogels with different contents of gelatin and glycerol. This result also demonstrates that the mechanical properties of the hydrogels can be simply tuned through controlled solvent evaporation (Figure 2f). The increase in normalized weight in air after 10 h indicates that the hydrogel with considerable glycerol has the ability to absorb moisture from the air with RH of 50%.[34] This ability is also confirmed by measuring the normalized weight of the hydrogel at ambient environment with constant RH. We find that the hydrogel reached the equilibrium state between dehydration and moisture absorption after 12 h; the equilibrated weight was determined by the RH of the environment (Figure S7, Supporting Information). After being placed in air for 30 days, the hydrogel still retains stable mechanical properties and considerable elasticity (Figure S8, Supporting Information); no failure or fracture is observed under 8000 or 3000 cyclic stretching with maximum strain of 20% and 50%, respectively (Figure S9, Supporting Information).

The as-prepared GA hydrogels have good stability, yet they are not stable in water due to the relatively weak noncovalent interactions that cannot resist the high osmotic pressure. The stability of the gelatin–alginate hydrogels in aqueous conditions can be increased by additional physical cross-linking of the alginate network by Ca^{2+} ions. This additional cross-linking affects not only the degradation performance, but also the mechanical properties of the hydrogels. As shown in Figure 2g, the mechanical properties of GA-20-3-0 hydrogel are significantly improved after incubation in 0.3 M calcium chloride ($CaCl_2$) solution for 1 day. E and σ_b of the hydrogel are slightly improved after being equilibrated in water for another 7 days to remove the residual Ca^{2+} ions. The content of alginate (f_y) has little influence on the mechanical properties of the as-prepared hydrogels, but markedly affects the properties of Ca^{2+}-cross-linked hydrogels (Figure S10, Supporting Information). To further quantitatively characterize the stability of Ca^{2+}-cross-linked hydrogel, the mechanical properties of the gel in GHS and PBS for 1 and 7 days are examined. The Ca^{2+}-cross-linked hydrogel shows almost the same mechanical properties (Figure 2h,i), whereas the gel without Ca^{2+} cross-linking completely degrades in GHS within 10 h (in Figure 1f). This result indicates that the additional cross-linking of Ca^{2+} ions significantly increases the stability of the biopolymer hydrogels and thereby favors applications in aqueous environments.

The biopolymer hydrogels also have moderate adhesion to various materials and biotissues, including glass, polypropylene, porcine skin, and rabbit heart (Figure S11, Supporting Information). The adhesiveness of the hydrogels may be attributed to their relatively low modulus and abundant active functional groups (e.g., carboxyl and amino groups) of the biopolymers. The former promotes better interfacial contact (and likely energy dissipation at the interface), and the latter facilitates the hydrogel to form noncovalent interaction with other materials.[35] Such moderate adhesiveness is essential for electronic skins by allowing the soft electronics to be attached on the skin without additional adhesives and to be removed without damaging the tissues.[36]

Another engaging feature of the HSE is the healability, which is favorable to increase the service lifetime of the electronics even after physical damage.[37] Healing of the biopolymer hydrogel is realized by sol–gel transition triggered by global or local heating near the damaged regions (**Figure 3**j). Laser is used as the heating source, which provides remote and spatial control of local temperature of the HSE. The laser irradiation can improve the fluidity of the hydrogel and LM, which triggers the self-healing of the damaged HSE to restore the original state and function (Figure S12, Supporting Information). Such healing of LM structures has been done with supramolecular polymers,[38] but not hydrogels. The healed hydrogel exhibits similar mechanical properties to the virgin one and does not break at the healed point during the tensile test (Figure 3k,l). Sophisticated structures such as Mobius ring can be constructed in the biopolymer hydrogel by harnessing this healing ability (Figure 3m). The assembly of biopolymer hydrogels to form special configurations may help to devise soft robots[39] and self-adaptive electronics.[40]

2.3. Hydrogel with Patterned Liquid Metal as Strain Sensor

Considering the excellent mechanical performances and self-adhesion property, the biopolymer hydrogels are ideal substrate materials to fabricate high-performance HSE by integrating patterned LM that has ultrahigh conductivity and deformability (Figure 3a). The glycerol-containing hydrogel is used for electronic skins, while the Ca^{2+}-cross-linked hydrogel for underwater electronics. The LM conductor serves as resistance-type strain sensor due to its sensitive resistance-response under deformation. To quantitatively characterize the sensing performance, a straight LM trace is printed on the hydrogel to detect mechanical strain. The relative resistance (R/R_0) of LM increases almost linearly with uniaxial deformation, and the gauge factor is about 0.55 (Figure 3b). The strain sensor can detect a small strain of 0.5% (Figure S13a, Supporting Information), which is comparable to most-existing resistance-type strain sensors.[3,8] Note that our strain sensor shows negligible electrical hysteresis during cyclic loading–unloading with a maximum strain of 50% due to the high resilience of GA hydrogel and the fast electrical response of LM (Figure S13b, Supporting Information). The strain sensor is stable under cyclic stretching (150 cycles) with a maximum strain of 50% in air (Figure 3c). Its sensing performance is rarely influenced by the stretching rate ranging from 100 to 400 mm min^{-1} (Figure S13c, Supporting Information). The baseline resistance slightly increases with the time, due to surface wrinkling of LM,[11,38] solvent evaporation, and fatigue of the hydrogel under cyclic loading.

The strain sensor has sufficiently high sensitivity to detect human facial micro-expression (e.g., frown) and tiny motions (e.g., jugular arterial pulse) when placed on the

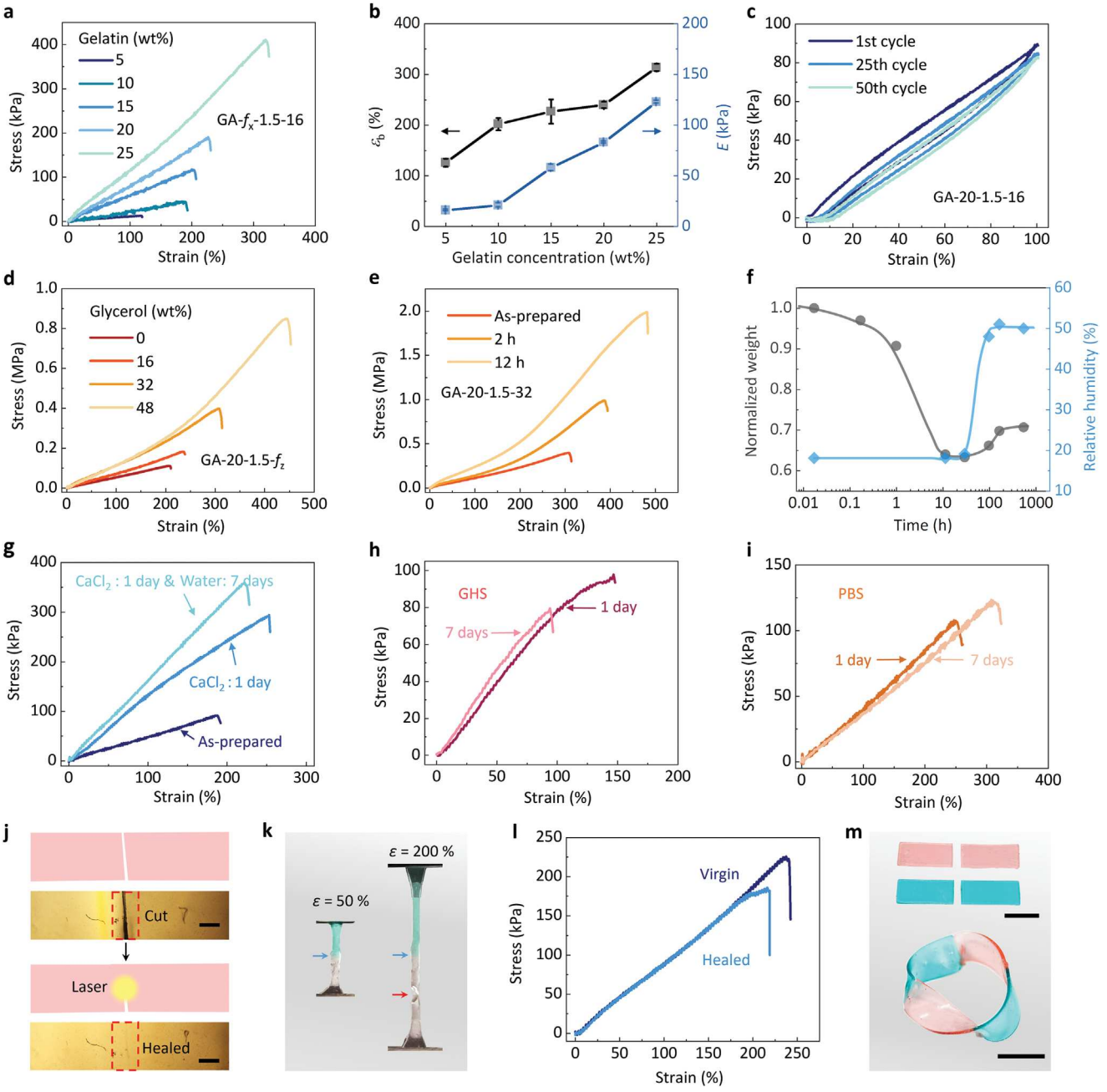

Figure 2. Tunable mechanical performances and healability of biopolymer hydrogels. a,b) Tensile stress–strain curves of the hydrogels with different content of gelatin (a) and corresponding strain at break (ε_b) and Young's modulus (E) (b). c) Cyclic loading–unloading of GA-20-1.5-16 hydrogel with maximum strain of 100%. d) Tensile stress–strain curves of the hydrogels with different content of glycerol. e) Stress–strain curves of GA-20-1.5-32 hydrogel after being placed in air for different time. f) Normalized weight of GA-20-1.5-32 hydrogel as a function of time after being placed in air at room temperature with varied relative humidity (RH). g) Tensile stress–strain curves of GA-20-3-0 hydrogel in as-prepared state, and after being incubated in 0.3 M $CaCl_2$ solution for 1 day, and then in water for another 7 days. h,i) Stress–strain curves of Ca^{2+}-cross-linked GA-20-3-0 hydrogel in GHS (h) and PBS (i) for 1 day and 7 days. j) Schematic and photos of laser-induced healing of GA-20-1.5-32 hydrogel. k) Healed dumbbell-shaped hydrogel sample was stretched to 50% and 200% strain. Blue arrow, healed point; red arrow, fracture point. l) Stress–strain curves of the gels in virgin state and healed state. m) 3D configuration (Mobius ring) of the hydrogel assembled by laser-induced healing. Error bars (standard deviation) are obtained from three parallel experiments. Scale bars = 1 cm.

skin (Figure 3d,e). In the magnified graph of Figure 3g, P-wave, T-wave, and D-wave can be clearly distinguished during one cardiac cycle, which reflect the health of the heart (Figure 3f). Because of the stable mechanical performance of Ca^{2+}-cross-linked hydrogel, the hydrogel device can also be used to detect the vibration of objects underwater. Inspired by the eardrum structure, the underwater electronics consist of a stiff gel frame (E = 100 MPa) that supports a soft biopolymer hydrogel with LM. The LM conductor can respond to slight vibration and produce resistance signal (Figure 3g). Different

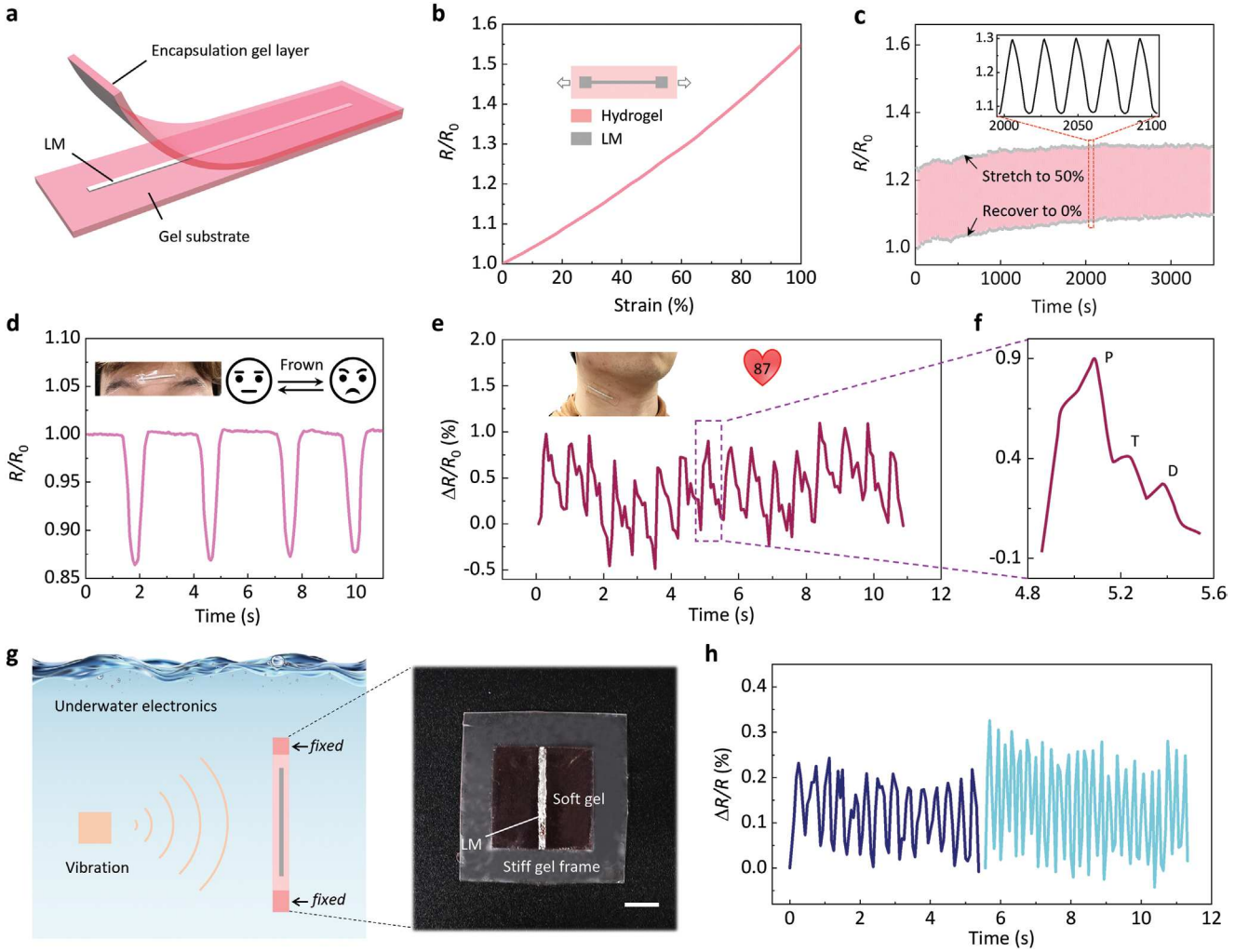

Figure 3. Hydrogel with patterned LM as strain sensor. a) Schematic for the generic structure of the strain sensor. b) Relative resistance change of the strain sensor as a function of applied tensile strain. c) Relative resistance change of the strain sensor under cyclic stretching with 50% strain in air (150 cycles). d) Strain sensor attached to the forehead of a volunteer to detect frown motion. e) Strain sensor attached to neck of volunteer to detect pulse. f) The magnified graph corresponding to one cardiac cycle with distinguishable P-wave, T-wave, and D-wave. g) Schematic of strain sensor as underwater electronics to detect vibration of objects. Scale bar = 1 cm. h) Relative resistance change of the underwater electronics responding to different vibration frequencies of an object with a distance of 5 cm.

vibration frequency of a glass plate underwater is accurately monitored by the resistance variation of the HSE (Figure 3h). Besides the resistance-type strain sensors, the facile printing of LM and easy fabrication of the GA hydrogel also enable the design of capacitance-type pressure sensor. As shown in Figure S14, Supporting Information, a 5 × 5 capacitance-type pressure sensor array is fabricated with the multilayer structure, which can detect the distribution of weight by measuring the relative capacitance change of the pixels of the pressure sensor array. These sensing performances suggest the potential applications of the HSE in healthcare monitoring and underwater communication.

2.4. Multifunctional HSE with Integrated Sensing Units

Imparting multiple functions to soft devices is important for practical applications in biomedical devices and soft robots. Although multifunctionality has been implemented in soft electronics with polymer films or elastomers as the substrates, it is challenging to develop multifunctional HSE with integrated sensing units due to the lack of conductive materials with high conductivity, good patternability, and high stretchability that can be assembled with hydrogel substrates. We devised multifunctional HSE with several sensing units that are connected by patterned LM, capable of simultaneously detecting human biophysical information (such as temperature, electrocardiogram [ECG], and pH) and controlling iontophoretic drug delivery (**Figure 4**a,b). The whole integrated HSE is encapsulated by another layer of biopolymer hydrogel except for the locations of sensing electrodes. Detailed fabrication process is described in Experimental Section.

The temperature sensor is prepared by connecting commercial negative temperature coefficient (NTC) temperature-sensitive resistor with two separated LM lines (Figure S15, Supporting Information). The resistance of the temperature sensor

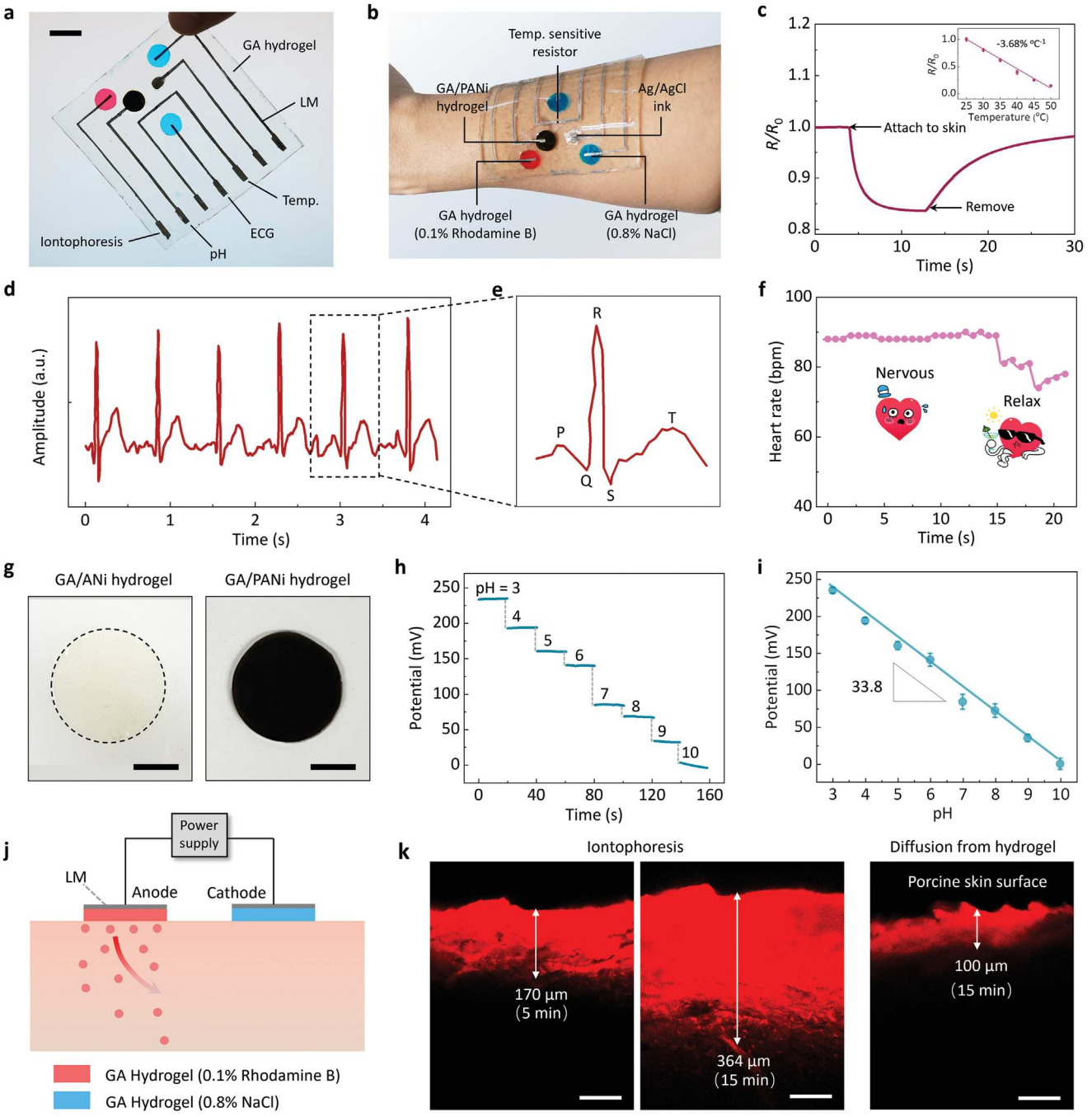

Figure 4. Multifunctional HSE with distributed sensing elements. a,b) Digital photos of the multifunctional HSE with distributed sensing units connected by patterned LM. Scale bar = 1 cm. c) Relative resistance change of temperature sensor after the attachment and removal of the HSE from the forearm of the volunteer. The inset shows the change of the resistance as a function of temperature. d,e) Biophysical signals recorded by ECG sensor consisted of GA/NaCl hydrogel working electrode measured from the forearm of the volunteer (d) and the magnified signal of a cardiac cycle (e). f) Instantaneous heart rates measured from the intervals of R–R peaks. g) Photos of gelatin–alginate hydrogels before and after polymerization to form the PANi network. Scale bars = 1 cm. h) Terraced variation of OCP with pH. i) Relationship between OCP and pH value. Error bars (standard deviation) are obtained from three parallel measurements. j) Schematic for iontophoretic drug delivery. k) Fluorescent micrographs of porcine skins via iontophoresis (left and mid) and natural diffusion (right). Scale bars = 100 µm.

decreases linearly (–3.68% $°C^{-1}$) with the increase in temperature. The resistance decreases by 23% and the temperature increases by 6.25 °C immediately when the HSE is attached to the forearm of a human volunteer; they subsequently recover to the original values after the removal of HSE from the skin (Figure 4c). The ECG sensor consists of disc-shape gelatin–alginate hydrogel with 0.8 wt% (relative to the total weight of hydrogel) sodium chloride (GA/NaCl) as working electrode and

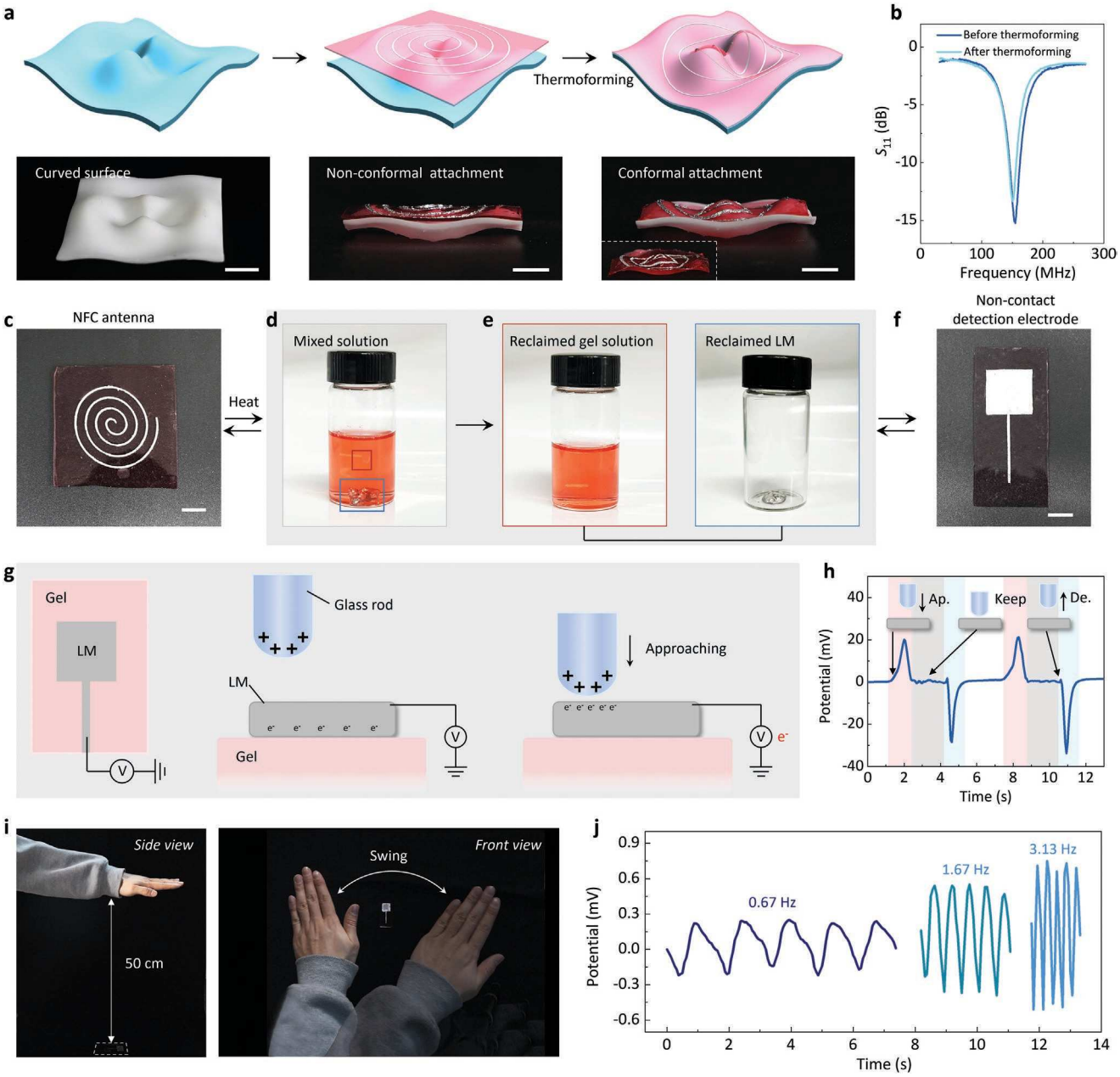

Figure 5. Temperature-mediated adaption and recyclability of the HSE. a) Schematic and digital photos of thermoforming process of the hydrogel to devise conformal HSE to set on curved surface. b) Return loss (S_{11}) of the LM antenna before and after the thermoforming. c–f) Recyclability of the HSE to devise new device with specific function. The hydrogel-LM antenna (c) is destructed at 60 °C for 30 min to separate the hydrogel (d) and the LM (e), which are reprocessed to another HSE for noncontact detection (f). g) Schematic for the working principle of noncontact detection. Variation of electrostatic field induced by a nearby object results in migration of electrons in LM, as well as between the LM and ground. h) Relative potential change in response of the approaching (AP.) and departure (De.) of a glass rod. i,j) Swing of the arm of a human volunteer above the device with different frequencies (i) and the corresponding change of potential (j). Scale bars = 1 cm.

two commercial silver/silver chloride (Ag/AgCl) gel electrodes as ground and reference electrodes (Figure S16, Supporting Information). Low-noise ECG signals can be collected with the GA/NaCl hydrogel working electrode, comparable to that of commercial Ag/AgCl gel working electrode (Figure 4d and Figure S17, Supporting Information). As shown in Figure 4e, the magnified graph of one cardiac cycle clearly shows P-wave, QRS complex, and T-wave. Moreover, instantaneous heart rates can be determined by the analysis of the intervals of R–R waves, which reflects a person's mental stress level at rest (Figure 4f). The pH sensor consists of GA/polyaniline (PANi) hydrogel as working electrode and Ag/AgCl ink as reference electrode (Figure 4g). The deprotonation of H^+ on the surface of GA/PANi hydrogel changes the open-circuit potential (OCP) between working and reference electrodes, which can be used to detect the pH values.[41] This pH sensor shows reliable

performance, as verified by the step decrease in OCP when pH changes from 3 to 10 (Figure 4h). A linear relationship is observed between OCP and pH, and the sensitivity of the pH sensor is −33.8 mV per decade of H^+ concentration (Figure 4i).

The porous structure of hydrophilic gel matrix allows facile loading and transport of molecules in hydrogel, which enables transdermal drug delivery.[42] For model iontophoretic drug delivery system,[43] two disc-shape GA hydrogel electrodes containing 0.1 wt% rhodamine B (relative to the total weight of hydrogel; served as the model drug) and 0.8 wt% NaCl are connected to the anode and the cathode by LM lines, respectively (Figure 4j). Under application of 1 V voltage, the diffusion depth of rhodamine B to pig skin is 173 µm after 5 min and 364 µm after 15 min, whereas the diffusion depth without electric voltage is only 100 µm after 15 min (Figure 4k). This result indicates that the HSE can afford controllable drug delivery to specific locations of underneath biotissues. We used low voltages (≈1 V) since higher voltages will result in electrochemical reduction of the oxide layer of the LM, and thus make the device unstable.[44] Although similar multifunctional soft electronics has been developed by utilizing elastomers as the substrate and serpentine rigid metal as the conductor,[45] there are no reports on HSE with distributed stretchable sensing units. The HSE with both detection and treatment abilities should find applications as smart wound dressing.[46]

2.5. Adaptability and Recyclability of the HSE

It is a challenge to wrap or conform 2D planar soft electronics on 3D curvilinear surfaces with non-Gaussian curvatures. Several strategies have been put forward to design conformal soft electronics by creating kirigami structure in soft electronics or using compliant ultrathin substrate,[47–49] but adding cuts or using ultrathin materials makes devices more prone to failure. Here we address this issue by affording the HSE with thermoforming capacity,[50] based on temperature-mediated sol–gel transition of the hydrogel substrate and high deformability of the patterned LM. As shown in **Figure 5**a and Figure S18, Supporting Information, the original planar HSE cannot be seamlessly attached to an irregular surface with non-Gaussian curvatures; only the convex locations of the substrate are in contact with the HSE. After placing the HSE together with the substrate in an oven of 60 °C for 5 min, the hydrogel softens and deforms seamlessly to the object. After peeling from the substrate, the HSE still maintains the 3D shape. Return loss (S_{11}) of the HSE with spiral shape LM line as near field communication (NFC) antenna[51] is measured by vector network analyzer before and after the thermoforming process, showing no obvious discrepancy in resonant frequency (frequency corresponding to the peak of S_{11}) or signal intensity (Figure 5b).

The temperature-triggered sol–gel transition of the biopolymer hydrogels and deformability of LM also allow reconstruction of the HSE to achieve different functions. As shown in Figure 5c, the structure of hydrogel-LM NFC antenna is deconstructed into its constituent materials at high temperature (60 °C) for 30 min (Figure 5d). With heating, the hydrogel becomes a viscous liquid and the LM aggregates and settles at the bottom of the container (Figure 5e and Figure S19, Supporting Information). These materials can be reclaimed and reused.

As shown in Figure 5f, the reconstructed HSE with LM electrode has the function to detect the motion of surrounding object in a noncontact way. This functional detection is realized by electrostatic-field-induced voltage of the nearby object.[52,53] As shown in Figure 5g, one test probe of a voltmeter is connected the LM electrode printed on the hydrogel and another probe is grounded. When a positive charged object (e.g., glass rod) is approaching the surface of LM, the free electrons in LM will move upwards because of the electrostatic attraction. Consequently, the electrons from the ground move to the LM, resulting in different potentials between the LM electrode and the ground that can be detected by the voltmeter. The value of potential recovers to its initial value after the migration of electrons is done. The departure of the glass rod causes the migration of electrons from the LM to the ground, which results in an opposite potential peak (Figure 5h). Therefore, by measuring the value change of the voltmeter, the motion of nearby objects can be detected in a noncontact way.

This HSE can also be used to detect human motion in real time, because human skin is usually charged. As shown in Figure 5i,j, the swinging arm of a human volunteer with different frequencies above the HSE with the distance of ≈50 cm can be clearly recorded by the voltmeter. Moreover, the relative location of the nearby object can be recognized by an array of LM electrodes. As shown in Figure S20, Supporting Information, four LM electrodes are printed on the biopolymer hydrogel. By measuring the variations of the potential of each electrode, one can distinguish the relative location of the vibrating glass rod. These results demonstrate our HSE has high modularity that is sustainable to reduce environment burden and malleable to self-adapt for different applications.

3. Conclusions

We have demonstrated a multifunctional HSE with various remarkable attributes by integrating biopolymer hydrogel, patterned LM, and multiple sensing units. The gelatin–alginate hydrogel has good mechanical properties, healability, biocompatibility, recyclability, and biodegradability, while the LM has high conductivity, good patternability, and recyclability. The resultant HSE has high sensitivity, good adaptability and recyclability, and versatile functions. It can serve as high-performance resistance-based strain sensor to detect tiny motion, such as the jugular arterial pulse. By integrating with sensing elements, the HSE possess multiple functions, is capable of detecting temperature, ECG signal, pH, and achieving controllable iontophoretic drug delivery. Owing to the temperature-mediated sol–gel transition of biopolymer hydrogel, the HSE has thermoforming capacity, facilitating seamless contact to objects with sophisticated geometries. We also demonstrate the recyclability the HSE to construct new device with specific functions. We believe that combining biopolymer hydrogel and printable LM is a promising strategy to develop modulable and sustainable soft electronics with multiple functions to reduce

environmental burden of electronic waste and achieve better human–computer interaction.

4. Experimental Section

Materials: Gelatin (porcine skin, type A, 300 g Bloom) and *N*,*N*,*N*′,*N*′-tetramethylethylenediamine were purchased from Sigma-Aldrich Co., Ltd. Methacrylamide (MAAm), methacrylic acid (MAAc), potassium persulfate (initiator), ammonium persulfate (APS, initiator), sodium chloride (NaCl), and rhodamine B were purchased from Aladdin Chemistry Co., Ltd. Alginate, $CaCl_2$, and glycerol were obtained from Sinopharm Chemical Reagent Co., Ltd. Aniline (ANi), and iron powder (diameter: 5 µm) were purchased from Macklin Co., Ltd. PBS was purchased from Dawen Biotechnology Co., Ltd. GHS was purchased from Yuanye Biotechnology Co., Ltd. LM alloy (74.5 wt% of gallium and 25.5 wt% of indium) was purchased from Dongguan Dingguan Metal Technology Co., Ltd. Ag/AgCl ink was purchased from ALS Co., Ltd. Millipore deionized water was used in all the experiments.

Fabrication of Gelatin–Alginate Hydrogels: The biopolymer hydrogels were facilely prepared by temperature-mediated sol–gel transition of mixed solution of gelatin, alginate, water, and glycerol. The recipes of precursor solutions for the hydrogels are listed in Table S2, Supporting Information. Prescribed amounts of gelatin and alginate were dissolved in deionized water or water/glycerol mixed solvent to obtain homogeneous solution in an oven of 60 °C for 6 h with stirring. Air bubbles in the solution were removed by placing the solution in a vacuum oven for 30 min. Subsequently, the precursor solution was poured into a reaction cell consisting of two glass substrates separated by silicone spacer, which was kept at room temperature for 24 h to obtain transparent hydrogel.

To regulate the stability and mechanical properties of the hydrogels, the as-prepared hydrogels were incubated in 0.3 M $CaCl_2$ solution for 24 h. The degradation time and mechanical properties could be modulated by controlling the incubation time to control the degree of physical cross-linking of the alginate network.

Degradation of the Biopolymer Hydrogels: To investigate the degradation property of the gelatin–alginate hydrogel, the hydrogels were incubated in the GHS at room temperature. The GHS was prepared by dissolving 0.1 g gelatin hydrolase in 100 mL deionized water. The state of the hydrogels was recorded by a digital camera.

Characterization of Mechanical Properties of the Biopolymer Hydrogels: To measure the mechanical properties of the hydrogels, dumbbell-shaped samples (width: 2 mm; gauge length: 12 mm) were obtained by a cutter. The experiments were performed by a commercial tensile tester (Instron 3343) with a constant stretching rate (100 mm min^{-1}) at room temperature in air. The Young's modulus of the hydrogels was calculated from the stress–strain curve with the strain below 5%.

Dehydration of the Hydrogels in Air: The disc-shaped as-prepared hydrogel (diameter: 25 mm; thickness: 1 mm) was placed in a watch glass in air; the normalized weight was defined by w/w_0, where the w and w_0 were the instantaneous and initial weight of the hydrogel, respectively. The RH of air was measured by a hygrometer (Xiaomi LYWSD03MMC).

Characterization of the Sol–Gel Transition Temperature of Biopolymer Hydrogels: To characterize the thermal stability of the hydrogels, the sol–gel transition temperature (T_{tans}) of the biopolymer hydrogels was characterized by a DHR-2 rheometer (TA Instruments). Disc-shaped hydrogel with a diameter of 25 mm and thickness of 1 mm was placed between the parallel plates of the rheometer. The edge of the hydrogel was sealed by liquid wax to reduce the evaporation of water in the hydrogels.[54] Temperature sweeps were performed at 1 Hz with a 2% strain amplitude. The sol–gel transition temperature, T_{tans}, was the temperature that the value of loss factor, tan δ was 1.

Adhesion and Peeling Tests: The pig skin was purchased from local market and the rabbit heart was obtained from Second Affiliated Hospital of Zhejiang University, Hangzhou, China, and the experiment was approved by the Committee on Animal Experimentation of Zhejiang University (accreditation number: 2019-959). All the materials were pretreated with isopropanol to remove the surface impurities for better interface contact between those materials and hydrogels. The hydrogel (GA-20-1.5-32) was slightly pressed on the surface of target materials at 50 °C for 30 s to soften the gel for adhesion. As shown in Figure S10, Supporting Information, one end of the hydrogel (50 mm × 10 mm × 1 mm) was clamped by the fixture of a commercial tester (Instron 3343) for peeling test with a peeling rate of 100 mm min^{-1}. The debonding energy (U_d) of the hydrogel with other materials was calculated by the formula of $U_d = F_p/W_0$, where F_p was the average peeling force at stable stage and W_0 was the width of the hydrogel sample.

Preparation of HSE with Patterned LM: The Fe-EGaIn was prepared by mixing 75 wt % EGaIn with 25 wt% iron power in centrifuge tube followed by oscillation at a speed of 2000 r min^{-1} for 60 s. The resultant viscous Fe-EGaIn amalgam could be patterned on various substrates by stencil printing method. Silhouetted mask (polyethylene terephthalate [PET]; thickness: 0.1 mm) with desired pattern was prepared by laser cutter. Then, the mask was placed atop the hydrogel (thickness: 0.5 mm) with gentle pressure. The Fe-EGaIn was applied on the mask with brush repeatedly. LM with complex pattern on the hydrogel was obtained after peeling off the mask. Another layer of gelatin–alginate hydrogel (thickness: 0.5 mm) was produced atop the hydrogel with patterned LM by sol–gel transition of gelatin–alginate solution for encapsulation to improve the stability of the HSE.

Fabrication and Characterization of Strain Sensor: To fabricate strain sensor as electronic skin to detect human motion, a straight LM line (40 mm × 2 mm × 0.2 mm) was printed on the GA-20-1.5-32 hydrogel (thickness: 0.5 mm) and followed with encapsulation by another layer of the same hydrogel (thickness: 0.5 mm). The corresponding dimensions of the device are shown in Figure S21, Supporting Information. The relative change of resistance (R/R_0) in the stretching process was measured with two probe method by a digital multimeter (Keysight Co., Ltd, 34465a), where the R and R_0 were the instantaneous resistance in stretching state and the initial resistance of the LM line, respectively.

The underwater electronics was fabricated by using stiff and tough poly(methacrylamide-*co*-methacrylic acid) [P(MAAm-*co*-MAAc)] hydrogel as the frame and soft gelatin–alginate hydrogel as the substrate of printed LM. The P(MAAm-*co*-MAAc) hydrogel was synthesized by free-radical copolymerization of MAAm and MAAc as described in the literature.[55] The hydrogel was cut to hollow square-shape by a laser cutter, and the dimensions of the gel is shown in Figure S21, Supporting Information. The following fabrication process was the same as the fabrication process of the electronic skins by replacing the GA-20-1.5-32 hydrogel with GA-20-3-0 hydrogel. The obtained device was incubated in 0.3 M $CaCl_2$ solution for 1 h to improve its stability in aqueous environment. The electrical stability of the underwater electronics was characterized by measuring the change of resistance of the device in air, water, and PBS (Figure S22, Supporting Information). The change of resistance of LM printed on the GA-20-1.5-32 hydrogel in powered state was also measured (Figure S23, Supporting Information). Stable performance was observed under 0.5 V potential more than 100 min and small increasement in resistance was observed under 1 V potential at 40 min.

Fabrication of Multifunctional HSE: The multifunctional HSE consists of three parts: stretchable biopolymer hydrogel substrate (GA-20-1.5-32; thickness: 1 mm), patterned LM conductor, and functional sensing electrodes (all the recipes of the precursor solutions for the fabrication of functional working electrodes are listed in Table S3, Supporting Information). Complex conducting circuits were obtained by stencil printing LM on the hydrogel substrate as described above. Then the functional hydrogel sensing electrodes and NTC temperature-sensitive resistor (bought from Alibaba Co., Ltd.) were placed on the predesigned position of the hydrogel substrate with pattern LM circuits. The Ag/AgCl reference electrode was fabricated by stencil printing of Ag/AgCl conductive ink on the PET substrate followed with drying in 60 °C oven for 2 h. Then the solidified Ag/AgCl electrode was peeled off the PET substrate and placed on the hydrogel substrate. For encapsulation, the precursor solution of GA-20-1.5-32 hydrogel was poured on the integrated soft electronics except for the regions of sensing electrodes.

pH sensor: The pH sensor consisted of gelatin–alginate (GA)/PANi working electrode and Ag/AgCl reference electrode. To fabricate GA/PANi hydrogel as the working electrode, 0.23 g of ANi, 2 g of gelatin, and 0.15 g of alginate were added to 7.85 g of water. The mixture was heated to 60 °C with stirring for 6 h to obtain homogeneous precursor solution (Table S3, Supporting Information). The subsequent steps were the same as the fabrication process of the biopolymer hydrogels without ANi. The as-prepared hydrogels with ANi were incubated in 2 M APS initiator solution for 2 h for the formation of PANi networks to obtain conductive GA/PANi hydrogels. Aqueous solution with different pH was prepared by the addition of HCl or NaOH. The solution was dripped on the HSE to fully cover the working and reference electrodes. The pH level of the solution was detected by measuring the OCPs between working electrode and reference electrode by a digital multimeter (Keysight Co., Ltd, 34465a). Before each test, the electrodes were rinsed with deionized water to remove the residual solution of last test.

ECG sensor: For the human experiments, all the demonstrations were performed at Department of Polymer Science and Engineering, Zhejiang University, China. The volunteer of the human experiments was the first author X.P.H. and he provide his consent for the publication of these pictures. Furthermore, the related project was fully assessed and approved by the ethics committee of the institute with permission from the participants. The ECG signals were recorded by a commercial ECG device (Heal Force PC-80D) with three electrode wires method. The ECG working electrode (GA/NaCl) was fabricated by incorporating 0.8 wt% of NaCl into the gelatin–alginate hydrogel (Table S3, Supporting Information). The integrated HSE containing ECG working electrode was attached to the right forearm of a human volunteer and two commercial Ag/AgCl gel electrodes were attached to the left forearm and right leg of the volunteer as reference electrodes and ground electrodes, respectively.

Iontophoretic Drug Delivery: Porcine skin was used as the model, which was pretreated with isopropanol to remove the surface impurities. The working electrode of the iontophoretic system was fabricated by incorporating 0.1 wt% of rhodamine B (relative to the hydrogel) into the GA-20-1.5-0 hydrogel. The reference electrode was fabricated by incorporating 0.8 wt% of NaCl into the GA-20-1.5-0 hydrogel (Table S3, Supporting Information). The integrated HSE was attached to the porcine skin with the working and reference electrodes connected to the anode and cathode, respectively, of the power supply with low voltages (≈1 V). For comparison, GA/0.1 wt% rhodamine B hydrogel was attached to the porcine skin without the electric field. After diffusion for a certain time (5 min or 15 min), the cross section of the porcine skin was observed by a confocal fluorescence microscope (Leica LSM780) to determine the diffusion depth of the rhodamine B.

Noncontact Detection: To realize noncontact detection, one probe of the digital multimeter (Keysight Co., Ltd, 34465a; served as voltmeter) was connected to the LM electrode printed on the hydrogel (GA-20-1.5-32) and another probe was grounded. A glass rod (diameter: 6 mm) charged by rubbing with cotton was used as detected object. The potential was recorded by the voltmeter when the glass rod approached and left the surface of LM electrode. To determine the relative location of the variation glass rod, four LM electrodes were printed on the hydrogel and the corresponding dimensions are shown in Figure S21, Supporting Information. The relative potential change of each LM electrode was recorded by the voltmeter. By analyzing the maximum potential change of each electrode, the location of the glass rod was distinguished qualitatively.

Supporting Information

Supporting Information is available from the Wiley Online Library or from the author.

Acknowledgements

The authors sincerely thank Meng Meng at University of Edinburgh for her help on drawing the schematic figures. Z.L.W. thanks the financial support from National Natural Science Foundation of China (51973189, 52173012). M.D.D. is grateful for support from the National Science Foundation (CMMI-2032409).

Conflict of Interest

The authors declare no conflict of interest.

Data Availability Statement

The data that support the findings of this study are available from the corresponding author upon reasonable request.

Keywords

biopolymer hydrogels, liquid metals, multifunctions, recyclability, soft electronics

Received: March 28, 2022
Revised: April 14, 2022
Published online: May 9, 2022

[1] Y. Liu, T. Yang, Y. Zhang, G. Qu, S. Wei, Z. Liu, T. Kong, *Adv. Mater.* **2019**, *31*, 1902783.
[2] J. C. Yang, J. Mun, S. Y. Kwon, S. Park, Z. Bao, S. Park, *Adv. Mater.* **2019**, *31*, 1904765.
[3] Y. Ohm, C. Pan, M. J. Ford, X. Huang, J. Liao, C. Majidi, *Nat. Electron.* **2021**, *4*, 185.
[4] J. Wang, M.-F. Lin, S. Park, P. S. Lee, *Mater. Today* **2018**, *21*, 508.
[5] H. Yuk, B. Lu, S. Lin, K. Qu, J. Xu, J. Luo, X. Zhao, *Nat. Commun.* **2020**, *11*, 1604.
[6] Y. Liu, J. Li, S. Song, J. Kang, Y. Tsao, S. Chen, P. M. George, Z. Bao, *Nat. Biotechnol.* **2020**, *38*, 1031.
[7] C. Keplinger, J.-Y. Sun, C. Foo, P. Rothemund, G. M. Whitesides, Z. Suo, *Science* **2013**, *341*, 984.
[8] Z. Lei, Q. Wang, S. Sun, W. Zhu, P. Wu, *Adv. Mater.* **2017**, *29*, 1700321.
[9] F. Zhu, S. Y. Zheng, J. Lin, Z. L. Wu, J. Yin, J. Qian, S. Qu, Q. Zheng, *J. Mater. Chem. C* **2020**, *8*, 7688.
[10] K. Li, X. Cheng, F. Zhu, L. Li, Z. Xie, H. Luan, Z. Wang, Z. Ji, H. Wang, F. Liu, Y. Xue, C. Jiang, X. Feng, L. Li, J. A. Rogers, Y. Huang, Y. Zhang, *Adv. Funct. Mater.* **2019**, *29*, 1806630.
[11] Z. J. Ma, Q. Xu, Q. Zhuang, X. Zhao, Y. Yang, H. Qiu, Z. Yang, C. Wang, Y. Chai, Z. Zheng, *Nat. Mater.* **2021**, *20*, 859.
[12] S. Liu, D. S. Shah, R. Kramer-Bottiglio, *Nat. Mater.* **2021**, *20*, 851.
[13] V. Vallem, E. Roosa, T. Ledinh, W. Jung, T.-i. Kim, S. Rashid-Nadimi, A. Kiani, M. D. Dickey, *Adv. Mater.* **2021**, *33*, 2103142.
[14] H. Wang, Y. Yao, Z. He, W. Rao, L. Hu, S. Chen, S. Dong, G. Chen, J. Liu, *Adv. Mater.* **2019**, *31*, 1901337.
[15] T. Shay, O. D. Velev, M. D. Dickey, *Soft Matter* **2018**, *14*, 3296.
[16] M. D. Dickey, *Adv. Mater.* **2017**, *29*, 1606425.
[17] J.-E. Park, H. S. Kang, M. Koo, C. Park, *Adv. Mater.* **2020**, *32*, 2002178.
[18] Y. Wang, G. A. Ameer, B. J. Sheppard, R. Langer, *Nat. Biotechnol.* **2002**, *20*, 602.
[19] C. Yang, Z. Suo, *Nat. Rev. Mater.* **2018**, *3*, 125.
[20] H. Yuk, B. Lu, X. Zhao, *Chem. Soc. Rev.* **2019**, *48*, 1642.
[21] Y. Zhou, C. Wan, Y. Yang, H. Yang, S. Wang, Z. Dai, K. Ji, H. Jiang, X. Chen, Y. Long, *Adv. Funct. Mater.* **2019**, *29*, 1806220.

[22] S. Lin, H. Yuk, T. Zhang, G. A. Parada, H. Koo, C. Yu, X. Zhao, *Adv. Mater.* **2016**, *28*, 4497.
[23] M. Baumgartner, F. Hartmann, M. Drack, D. Preninger, D. Wirthl, S. Hild, S. Bauer, M. Kaltenbrunner, *Nat. Mater.* **2020**, *19*, 1102.
[24] H. C. Yu, H. Zhang, K.-F. Ren, Z. Ying, F. Zhu, J. Qian, J. Ji, Z. L. Wu, Q. Zheng, *ACS Appl. Mater. Interfaces* **2018**, *10*, 9002.
[25] D. Gao, J. Lv, P. S. Lee, *Adv. Mater.* **2022**, *34*, 2105020.
[26] Y. Choi, K. Park, H. Choi, D. Son, M. Shin, *Polymers* **2021**, *13*, 1133.
[27] S. R. Derkach, N. G. Voron'ko, N. I. Sokolan, D. S. Kolotova, Y. A. Kuchina, *J. Dispersion Sci. Technol.* **2019**, *41*, 690.
[28] K. B. Djagny, Z. Wang, S. Xu, *Crit. Rev. Food Sci. Nutr.* **2001**, *41*, 481.
[29] K. Y. Lee, D. J. Mooney, *Prog. Polym. Sci.* **2012**, *37*, 106.
[30] A. S. Sharova, F. Melloni, G. Lanzani, C. J. Bettinger, M. Caironi, *Adv. Mater. Technol.* **2021**, *6*, 2000757.
[31] A. Cook, D. P. Parekh, C. Ladd, G. Kotwal, L. Panich, M. Durstock, M. D. Dickey, C. E. Tabor, *Adv. Eng. Mater.* **2019**, *21*, 1900400.
[32] R. Guo, X. Sun, B. Yuan, H. Wang, J. Liu, *Adv. Sci.* **2019**, *6*, 1901478.
[33] M. Thomazine, R. A. Carvalho, P. J. A. Sobral, *J. Food Sci.* **2005**, *70*, E172.
[34] K. Matsumoto, N. Sakikawa, T. Miyata, *Nat. Commun.* **2018**, *9*, 2315.
[35] Y. Ma, B. Zhang, I. Frenkel, Z. Zhang, X. Pei, F. Zhou, X. He, *Rev. Adhes. Adhes.* **2020**, *9*, 167.
[36] G. Li, K. Huang, J. Deng, M. Guo, M. Cai, Y. Zhang, C. F. Guo, *Adv. Mater.* **2022**, *34*, 220026.
[37] J. Kang, J. B.-H. Tok, Z. Bao, *Nat. Electron.* **2019**, *2*, 144.
[38] E. Palleau, S. Reece, S. C. Desai, M. E. Smith, M. D. Dickey, *Adv. Mater.* **2013**, *25*, 1589.
[39] Z.-Z. Nie, B. Zuo, M. Wang, S. Huang, X.-M. Chen, Z.-Y. Liu, H. Yang, *Nat. Commun.* **2021**, *12*, 2334.
[40] X. P. Hao, C. Y. Li, C. W. Zhang, M. Du, Z. Ying, Q. Zheng, Z. L. Wu, *Adv. Funct. Mater.* **2021**, *31*, 2105481.
[41] T. Guinovart, G. Valdés-Ramírez, J. R. Windmiller, F. J. Andrade, J. Wang, *Electroanalysis* **2014**, *26*, 1345.
[42] M. R. Prausnitz, R. Langer, *Nat. Biotechnol.* **2008**, *26*, 1261.
[43] C. Wu, P. Jiang, W. Li, H. Guo, J. Wang, J. Chen, M. R. Prausnitz, Z. L. Wang, *Adv. Funct. Mater.* **2020**, *30*, 1907378.
[44] M. R. Khana, C. B. Eakera, E. F. Bowdenb, M. D. Dickey, *Proc. Natl. Acad. Sci. U. S. A.* **2014**, *111*, 14047.
[45] G. Xu, Y. Lu, C. Cheng, X. Li, J. Xu, Z. Liu, J. Liu, G. Liu, Z. Shi, Z. Chen, F. Zhang, Y. Jia, D. Xu, W. Yuan, Z. Cui, S. S. Low, Q. Liu, *Adv. Funct. Mater.* **2021**, *31*, 2100852.
[46] C. Wang, E. S. Sani, W. Gao, *Adv. Funct. Mater.* **2022**, *32*, 2111022.
[47] H. C. Yu, X. P. Hao, C. W. Zhang, S. Y. Zheng, M. Du, Z. L. Wu, Q. Zheng, *Small* **2021**, *17*, 2103836.
[48] X. P. Hao, Z. Xu, C. Y. Li, W. Hong, Q. Zheng, Z. L. Wu, *Adv. Mater.* **2020**, *32*, 2000781.
[49] Y. Zhao, B. Zhang, B. Yao, Y. Qiu, Z. Peng, Y. Zhang, Y. Alsaid, I. Frenkel, K. Youssef, Q. Pei, X. He, *Matter* **2020**, *3*, 1196.
[50] J. Choi, C. Han, S. Cho, K. Kim, J. Ahn, D. D. Orbe, I. Cho, Z.-J. Zhao, Y. S. Oh, H. Hong, S. S. Kim, I. Park, *Sci. Adv.* **2021**, *7*, eabj0694.
[51] K. Yamagishi, W. Zhou, T. Ching, S. Y. Huang, M. Hashimoto, *Adv. Mater.* **2021**, *33*, 2008062.
[52] W. J. Song, Y. Lee, Y. Jung, Y.-W. Kang, J. Kim, J.-M. Park, Y.-L. Park, H.-Y. Kim, J.-Y. Sun, *Sci. Adv.* **2021**, *7*, eabg9203.
[53] L. Lu, C. Jiang, G. Hu, J. Liu, B. Yang, *Adv. Mater.* **2021**, *33*, 2100218.
[54] H. C. Yu, S. Y. Zheng, L. Fang, Z. Ying, M. Du, J. Wang, K.-F. Ren, Z. L. Wu, Q. Zheng, *Adv. Mater.* **2020**, *32*, 2005171.
[55] Y. J. Wang, X. N. Zhang, Y. Song, Y. Zhao, L. Chen, F. Su, L. Li, Z. L. Wu, Q. Zheng, *Chem. Mater.* **2019**, *31*, 1430.